Journal of Materials and Electronic Devices 4 (2024) 36-45


# Current–Voltage Characteristics of Al/(CdO:ZnO:NiO:Ti)/p-Si/Al Quaternary Functional Schottky Diodes

Erdal KARAKUŞ[1], Çiğdem Şükriye GÜÇLÜ[2], Mümin Mehmet KOÇ[1,3], Burhan COŞKUN[1*]

[1]Kırklareli University, Faculty of Art and Science, Department of Physics, Kırklareli, Türkiye
[2] Gazi University, Faculty of Sciences, Department of Physics, Ankara, Türkiye
[3] Kırklareli University, School of Medical Service, Kırklareli, Türkiye

Solutions containing CdO:ZnO:NiO:Ti nanoparticle complex were produced in using sol gel method. CdO:ZnO:NiO:Ti solutions were drop cast p type Si wafer and thin films were obtained. I-V characteristics of Al/(CdO:ZnO:NiO:Ti)/p-Si/Al photodiodes were obtained using Fytronix solar simulator. Using the I-V data various diode characteristics pertaining to Al/(CdO:ZnO:NiO:Ti)/p-Si/Al photodiodes were calculated such as barrier height, ideality factor, saturation constants. In investigations, various methods were used such as thermionic emission theory, Cheung & Cheung method and Norde method. Photo responsive characteristics of the diodes revealed that thin films show photo responsive. Barrier height of the Al/(CdO:ZnO:NiO:Ti)/p-Si/Al Quaternary Functional Schottky Diodes were found to be 0.73 eV and 0.69 eV for the measurements conducted in dark and under illumination, respectively. Ideality factors of the diodes were found to be 9.61 and 8.78 for the measurements in dark and under illumination. Series resistance and Shunt resistance values were also evaluated using alternative methods.

***Keywords:*** *Quaternary Photodiodes; Al/(CdO:ZnO:NiO:Ti)/p-Si/Al; Schottky Diodes; CdO; ZnO*

*Submission Date: 09 September 2024*
*Acceptance Date: 10 October2024*

**Corresponding author: burhan.coskun@klu.edu.tr*

## 1. Introduction

Thin films are vastly used in different nanotechnology applications. Thin films have attracted considerable interest in the field of materials science due to their wide-ranging applications in electronics, optoelectronics, and energy technologies[1]. These materials, characterized by thicknesses that can range from a few nanometers to several micrometers, display distinct properties that set them apart from their bulk forms [1]. Notable among these properties are their high surface-to-volume ratios, adjustable optical and electronic features, and mechanical flexibility, which make them well-suited for various contemporary technological uses [2]. Thin films can be categorized into several types, including metallic, organic, and hybrid materials, based on their composition and structural characteristics. Metallic thin films, which are primarily made of metals or their alloys, are recognized for their excellent electrical conductivity, optical characteristics, and mechanical strength. These films find extensive application in microelectronics, sensors, and photovoltaics due to their outstanding thermal and electrical properties[3–6]. For example, zinc oxide (ZnO) thin films are noted for their remarkable properties, such as high electron mobility and chemical stability, making them ideal for use in sensors and optoelectronic devices[7–9]. Organic thin films, composed of polymers or organic molecules, are distinguished by their flexibility, light weight, and cost-effectiveness, rendering them particularly suitable for flexible electronics and organic light-emitting diodes (OLEDs). Hybrid thin films, which integrate both inorganic and organic materials, capitalize on the benefits of both types, offering tunable properties for multifunctional applications[10–12]. The exceptional electrical conductivity of metallic thin films is particularly valued, as it is essential

for the creation of electronic circuits, electrodes[13,14]. Their high reflectivity and optical absorption capabilities also make them suitable for use in photodetectors, solar cells, and reflective coatings [15–17]. Additionally, metallic thin films demonstrate remarkable thermal stability and resistance to corrosion, which enhances their durability in challenging environments—an important factor for optoelectronic applications such as light-emitting diodes and lasers.

Among the metallic thin films, those made from cadmium (Cd), zinc (Zn), nickel (Ni), and titanium (Ti) are particularly noteworthy due to their unique characteristics and versatile applications[18–24]. Cadmium-based thin films, like cadmium oxide (CdO), are recognized for their high transparency and electrical conductivity, making them ideal for transparent conducting electrodes in solar cells and display technologies[21,24,25]. Zinc-based thin films, such as zinc oxide (ZnO), are celebrated for their excellent optical transparency, piezoelectric properties, and wide bandgap, which enable their use in UV photodetectors and gas sensors[7,8,26]. Nickel-based thin films, including nickel oxide (NiO), exhibit p-type semiconducting behavior and good chemical stability, making them valuable for applications in electrochromic devices and batteries[27]. Titanium-based thin films, especially titanium dioxide ($TiO_2$), are renowned for their photocatalytic properties and biocompatibility, facilitating their use in self-cleaning coatings and photovoltaic systems[28].

Quaternary thin films, which are created by combining four different elements or compounds, represent a sophisticated class of materials that provide enhanced flexibility in adjusting their optical, electrical, and structural properties. These materials are particularly significant for achieving multifunctional performance, making them suitable for advanced sensors and energy harvesting systems. Notable examples include CdZnTeSe (cadmium-zinc-tellurium-selenium) for photovoltaic applications and $CuInGaSe_2$ (copper-indium-gallium-selenide) for thin-film solar cells, both of which demonstrate excellent absorption coefficients and high efficiency in light absorption and energy conversion[29–32]. Previously, $Cu_2NiSnS_4$ and $Cu_2CoSnS_4$ diodes were reported by our group which exhibit outstanding infrared sensing capabilities and good electronic and optoelectronic characteristics[33,34].

Schottky diodes that utilize quaternary thin films, such as CdO:ZnO:NiO:Ti, have attracted significant interest due to their superior electronic and optoelectronic properties. These structures combine the strengths of each constituent material, offering tunable bandgaps and improved charge carrier mobility. The integration of various oxides in these diodes enhances the Schottky barrier height, facilitating better charge injection and transport, which is critical for applications in flexible electronics and transparent circuits.

Thin films, particularly those that are metallic and quaternary in nature, have transformed the field of materials science by providing tailored properties for a wide array of applications. The investigation of Cd-, Zn-, Ni-, and Ti-based thin films highlights their adaptability in electronic and optoelectronic technologies[27,28,35-37]. As the demand for compact and multifunctional devices continues to rise, the research and refinement of thin film materials will be essential in shaping future technological advancements.

In this report, I-V characteristics of CdO:ZnO:NiO:Ti thin films were assessed using various investigation methods. Various parameters were assessed such as barrier height, ideality factor, shunt resistance, series resistance, saturation current using various methods such as thermionic emission theory, Cheung&Cheung and Norde methods. It was seen CdO:ZnO:NiO:Ti structures exhibit Schottky diode like characteristics and responsive to light.

## 2. Experimental

Al/(CdO:ZnO:NiO:Ti)/p-Si/Au (MIS) structures were fabricated on a p-Si wafer that was 300 μm thick, <100> float-zone, with a resistivity of 1–10 cm-Ω and polished on one side. Prior to the fabrication process, the p-Si wafer underwent cleaning process. Sonication was applied to the p type silicon wafers for 5 mins in deionized water. Si wafer then sonicated in ethanol for 5 mins and sonicated in deionized water. Lastly, HF:$H_2O$ (1:10ml) were prepared and sonicated for 5 mins and washed using pure water. Samples were then dried using $N_2$ gas. 2 cm x 2 cm wafers were cut; 6 layers of film were then spin coated on substrates. Spin coating was applied at 3000 rpm for 30 secs for each layer. Each layer was dried on a hot Subsequently, the wafer was transferred to a vacuum chamber where high-purity gold (99.999%) with a thickness of 150 nm was thermally evaporated onto the backside of the p-Si wafer using a high-vacuum metal evaporation system at a pressure of $10^{-6}$ Torr. The wafer was then annealed at 500 °C in a nitrogen atmosphere to achieve low-resistivity and good ohmic contact. Next, the prepared (CdO:ZnO) solution was applied to the front of the p-Si wafer as an interfacial layer using the spin-coating technique. This solution was created by separately dissolving zinc acetate ($Zn(CH_3COO)_2$) and nickel chloride ($NiCl_2$) in 15 ml of methoxyethanol to produce 0.1 M solutions of zinc and nickel, respectively. Additionally, a 0.4 M base solution was prepared by dissolving NaOH in 65 ml of methanol. The synthesis of ZnO and Cd involved agitating the 0.1 M zinc solution and the 0.4 M base solution separately for 10 minutes at 500 rpm, with ethanolamine serving as a stabilizer. The coated films were then dried for one hour at 50 °C on a hot plate to form solid films. For further modification, PCBM, a fullerene derivative, was coated onto the front of the p-Si wafer for 30

seconds at 2000 rpm and 80 °C using a Fytronix spin coater system. The temperature of 80 °C was crucial for achieving optimal coating characteristics for the layer, allowing for the formation of a highly homogeneous layer with improved adhesion to the substrate. After the coating process, PCBM was dissolved in chlorobenzene. Finally, high-purity aluminium with a diameter of 1 mm and a thickness of 150 nm was deposited onto the (Cd:ZnO) interlayer using the same thermal evaporation system. The thickness of both the rectifier Al Schottky contacts and the backside Au ohmic contacts, as well as their deposition rates, were monitored using a quartz crystal metal thickness meter. For electrical measurements, thin silver-coated wires were employed as the electrode connection system, and the fabricated samples were mounted on a copper holder. Characterization measurements, including capacitance-voltage (C-V) and conductance-voltage (G/-V) measurements, were performed using the Fytronix-FY-7000 characterization system within a Fytronix cryostat at approximately $10^{-3}$ Torr to minimize external effects. Data acquisition and analysis were conducted using a software program, Silicon (2024), along with an IEEE-488 ac/dc converter card. A schematic diagram of the Al/(CdO:ZnO:NiO:Ti)/p-Si/Al diodes is shown in Figure 1. All device characterization equipment was provided by Fytronix.

## 3. Results

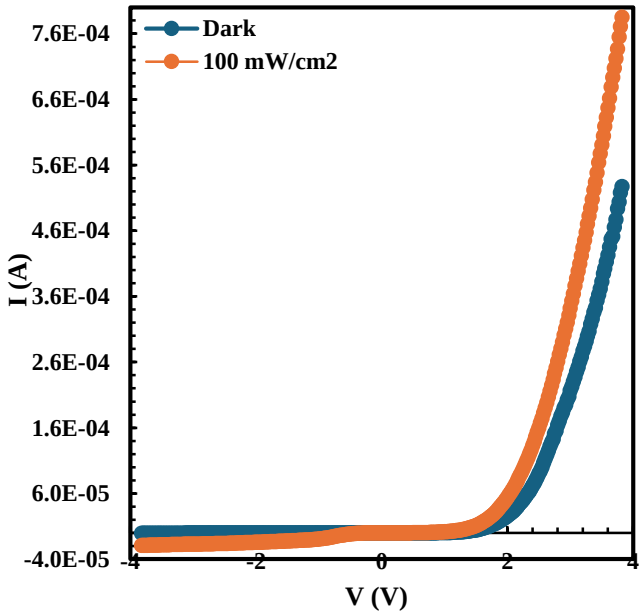


**Figure 1:** Metric I-V characteristics of Al/(CdO:ZnO:NiO:Ti)/p-Si/Al diodes obtained under dark and 100mW/cm$^2$ illumination.

The current-voltage (I-V) characteristics of the fabricated Al/(CdO:ZnO:NiO:Ti)/p-Si/Al quaternary functional Schottky-type photodiodes are illustrated in Figure 1, showcasing both dark and illuminated states at a light intensity of 100 mW·cm$^{-2}$. The I-V curves for forward and reverse bias were displayed on both linear and semi-logarithmic scales across a voltage range of ±4V. In the dark, the current in both forward and reverse bias regions increases as the voltage rises. However, when illuminated, the reverse bias current is markedly greater than the forward bias current. This phenomenon occurs because, during reverse bias, the internal and external electric fields align in the same direction, which amplifies the overall electric field at the junction (E+ε). As a result, electron-hole pairs generated by incident photons in the junction area are prevented from recombining and neutralizing due to the strong electric field. Instead, these charge carriers are driven in opposite directions by the force $\mathbf{F} = \pm q\Sigma\mathbf{E} = \pm q(\mathbf{E}+\boldsymbol{\varepsilon})$, leading to a net photocurrent in the circuit.

Conversely, in the forward bias scenario, the internal and external electric fields counteract each other, resulting in increased recombination and neutralization of electron-hole pairs, which ultimately diminishes the photocurrent.

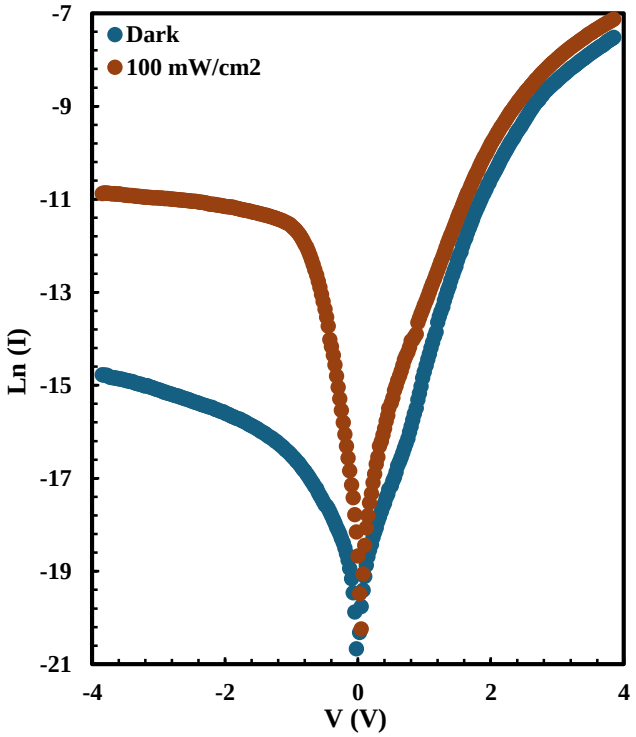


**Figure 2:** Semi-logarithmic I-V characteristics of Al/(CdO:ZnO:NiO:Ti)/p-Si/Al diodes obtained in dark and 100mW.cm$^{-2}$ illumination.

As seen in Figure 2, the semi-logarithmic forward bias $\ln I_F$-$V_F$ graphs exhibit a distinct linear region in the mid-voltage ranges under both dark and illuminated conditions. Additionally, as observed from the figure, the absence of a smooth or clear saturation in the reverse bias region can be attributed to several factors, including a reduction or decrease in the Schottky barrier height due to image force effects, interface states/traps, and the presence of a natural

or intentionally grown interfacial layer between the metal and semiconductor.

However, as the voltage increases into the high-voltage region, deviations from linearity occur due to the effects of both the series resistance ($R_s$) and the (CdO:ZnO:NiO:Ti) interfacial layer [1–3, 24–28].

In a MIS-type diode with an interfacial layer, if the ideality factor is greater than 1 and the series resistance (Rs) is not negligibly small, the relationship between current (I) and voltage (V) under forward bias (V ≥ 3kT/q) is given by Equation 1 [38–40].

$$I = I_0 \exp\left(\frac{qV - IR_S}{nkT}\right)\left[1 - \exp\left(\frac{-q(V - IR_S)}{kT}\right)\right] \quad (1)$$

In Equation 1, $I_o$ represents the saturation current, $I_{RS}$ denotes the voltage drop across $R_S$, T is the temperature in Kelvin, k is the Boltzmann constant, and the other quantities are well-known in the literature.

At moderate voltage values, the $IR_S$ term is sufficiently small compared to the applied voltage on the diode and can be neglected.

The explicit expression for $I_o$, the reverse bias saturation current, is provided below in Equation 2.

Such a case also supports the case that thin films can be used in photodetector and solar detector applications. Using absorbance data, $E_g$ (energy band gap) of the thin films were determined. Following formula was used in the calculations

$$I_0 = AA^*T^2\, exp\left(-\frac{q\varphi_{b0}}{kT}\right) \quad (2)$$

In this case, by taking the logarithm of both sides of Equation 1 and rearranging it, a linear equation as given in Equation 2 is obtained.

$$\ln(I) = \ln(I_0) + \frac{q}{nkT}V_D \quad (3)$$

The ideality factor of the diode and the ln($I_o$) values were obtained, respectively, from the slope of the ln(I)-V graph in the positive region (tanθ = q/nkT) under both dark conditions and a light intensity of 100 mW·cm$^{-2}$, and by fitting to the current axis at 0 V using Equation 3.

$$n = \frac{q}{kTtan\theta} \quad (4)$$

Thus, the potential barrier height ($\Phi_{Bo}$) of the diode at zero bias was calculated for both dark conditions and under illumination intensity of 100 mW·cm$^{-2}$ using the obtained $I_o$ and the rectifying contact area (A) of the diode, along with Equation 2, as shown in Equation 5 below.

$$q\Phi_{B0} = kT\, ln\left(\frac{AA^*T^2}{I_0}\right) \quad (5)$$

In general, the ln(I)-V graph of Schottky diodes is expected to show a linear relationship in the forward bias region. However, in practice, at higher positive voltages (V ≥ 1V), the ln(I)-V curve deviates significantly from linearity because of series resistance and the interfacial layer. The actual series and shunt resistances ($R_s$, $R_{sh}$) of semiconductor devices correspond to the extreme forward and reverse voltage values, respectively ($R_i = V_i/I_i \pm V_i$). Therefore, these values were obtained from the resistance ($R_i$) values calculated as a function of voltage using Ohm's Law, and the results are presented in Figure 3.

**Figure 3:** $R_i$-$V_i$ curves of Al/(CdO:ZnO:NiO:Ti)/p-Si/Al diodes obtained in dark and 100mW.cm$^{-2}$ illumination.

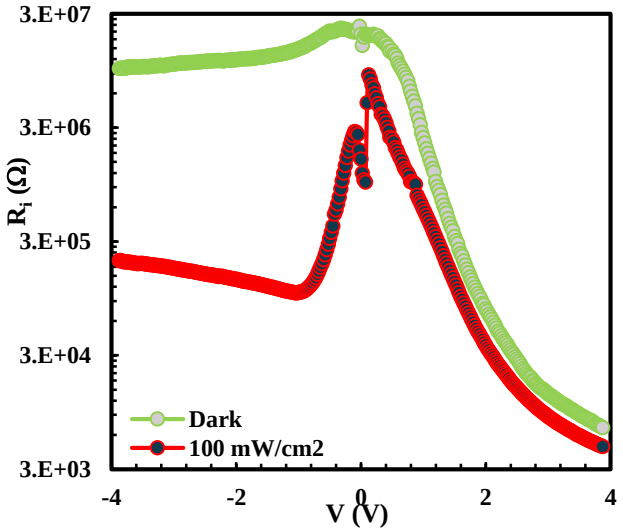


As seen in the figure, the $R_i$-V curves remain nearly constant, i.e., independent of voltage, within the ±4V range, which corresponds to the actual $R_s$ and $R_{sh}$ values of the diode.

Metal-semiconductor (MS) or metal-insulator-semiconductor (MIS) type semiconductor devices/diodes are expected to conduct under forward bias but exhibit negligible current under reverse bias. However, in practice, this behaviour often deviates. For ideal diodes, the rectification ratio (RR = $I_F/I_R$) at a fixed ±V value is typically on the order of 10$^9$.

In this study, this value was determined at ±4V under both dark conditions and a light intensity of 100 mW/cm², and the results are provided in Table 1.

**Table 1:** Essential electrical parameters ($I_0$, $\Phi_{B0}$, n, $I_0$, $R_s$, $R_{sh}$, RR) and values obtained for Al/(CdO:ZnO:NiO:Ti)/p-Si/Al diodes for both dark and illumination under 100mW.cm$^{-2}$ at room temperature.

| | $I_0$ (A) | n | $\Phi_{B0}$ (eV) | $R_s$(4V) (kW) | $R_{sh}$ (-4V) (MW) | RR |
|---|---|---|---|---|---|---|
| **Dark** | $4.643x10^{-9}$ | 9.61 | 0.73 | 6.50 | 10.00 | 1540 |
| **100mW/cm²** | $2.330x10^{-8}$ | 8.79 | 0.69 | 4.44 | 0.207 | 46.99 |

As seen in Table 1, the n values obtained under both dark conditions and a light intensity of 100 mW·cm$^{-2}$ are significantly higher than the ideal value of 1. As indicated in Equation 6, this behaviour is directly proportional to the thickness of the interfacial layer and the density of interface states, while it is inversely proportional to the dielectric constant of the interfacial layer and the depletion region width.

In the literature, this phenomenon is generally attributed to the presence of interface states, the existence of an interfacial layer, and the inhomogeneity of the potential barrier formed between the metal and the semiconductor [38–40]. In Equation 6, δ represents the thickness of the interfacial layer, $W_D$ is the width of the depletion region, and $\varepsilon_s$ and $\varepsilon_i$ are the dielectric constants of the semiconductor and the interfacial layer, respectively.

$$n(V) = (qV/kT)Ln(I/I_0) = 1 + \frac{d_i}{\varepsilon_i}\left[\frac{\varepsilon_s}{W_D} + qN_{SS}(V)\right] \quad (6)$$

An alternative method for calculating the fundamental diode parameters, such as n, $R_S$, and $\Phi_B$, was developed by Cheung and Cheung. This method is applicable for sufficiently high positive voltages (the region where the ln(I)-V curve begins to deviate from linearity) and utilizes the two equations provided below [41].

$$\frac{dV}{d\ln I} = IR_S + \left(\frac{nkT}{q}\right) \quad (6a)$$

$$H(I) = V - \frac{nkT}{q}\ln\left(\frac{1}{AA^*T^2}\right) = IR_S + n\Phi_B \quad (6b)$$

Using Equations 6a and 6b, the dV/dln(I) - V and H(I)-V graphs were obtained for both dark conditions and under 100 mW/cm$^{-2}$ illumination and are presented in Figure 4 and 5.

As can be clearly seen in Figure 4 and 5 both the dV/dln(I)-V and H(I) - V graphs exhibit a well-defined linear region over a wide range of voltage and current values under both dark and illuminated conditions.

According to Equations 6a and 6b, the slope of the dLn(I)-I and H(I)-V graphs directly provide the $R_s$ value, while the intercepts correspond to nkT/q and n$\Phi_B$, respectively.

Thus, the n value calculated from Equation 6a (using n= (q/kT)/slope) was substituted into Equation 6b. From the slope of the resulting H(I) - I graph, the $\Phi_B$ value ($\Phi_B$= intercept/n) was calculated. These results are summarized in Table 2.

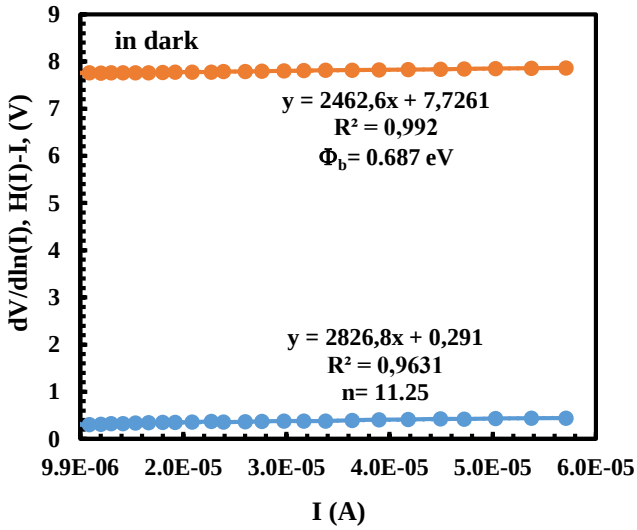


**Figure 4:** dV/dln(I) - V & H(I) - V curves of Al/(CdO:ZnO:NiO:Ti)/p-Si/Al diode obtained in the dark.

As seen in the table, the obtained n, $R_S$, and $\Phi_B$ values are highly dependent on the illumination intensity, like those derived from TE theory. However, some differences between them indicate that the calculation method used and their dependence on voltage play a significant role[42–45].

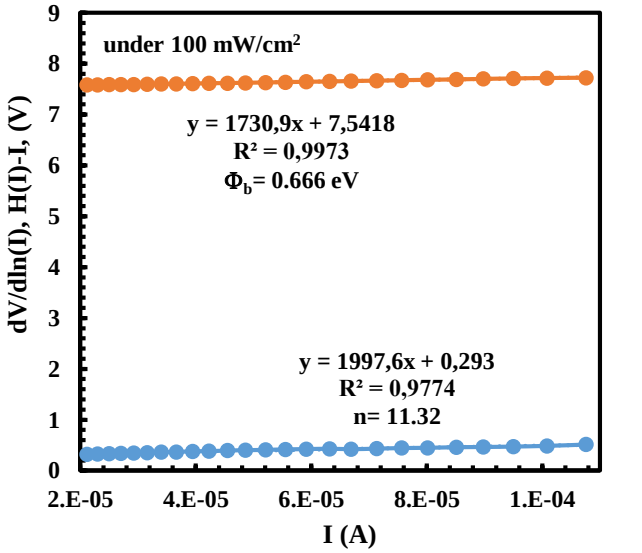


**Figure 5:** dV/dln(I)-V & H(I)-V curves of Al/(CdO:ZnO:NiO:Ti)/p-Si/Al diode obtained in the under 100mW.cm$^{-2}$ light intensity.

Both $R_S$ and $\Phi_B$ values can also be calculated using the equations developed by Norde, which are provided below. According to Norde, when the ln(I)-V curves do not exhibit a distinct linear region, the relationship between current and voltage can be described using Equation 7 based on TE theory [2,3].

$$F(V) = \frac{V}{\gamma} - \frac{kT}{q}\left[\ln\left(\frac{I(V)}{AA^*T^2}\right)\right] \quad (7)$$

$$R_s = \frac{kT(\gamma - n)}{qI_o} \quad (8a)$$

$$\Phi_B = F_o + \frac{V_o}{\gamma} - \frac{kT}{q} \quad (8b)$$

In Equation 7, the arbitrary constant γ must be chosen to be greater than the ideality factor value obtained from TE theory. Using Equation 7, the F(V)-V curves were obtained under both dark and illuminated conditions, and these are presented in Figure 6.

As clearly shown in Figure 6, the F(V)-V graphs exhibit a distinct minimum point under both dark and illuminated conditions. Using the values corresponding to this minimum point ($F_0$) as well as the associated $V_0$ and $I_0$ values, $R_S$ and $\Phi_B$ were calculated as a third method using Equations 4.8a and 4.8b. The results were presented in Table 2, along with those obtained from the Cheung functions.

When both Table 1 and Table 2 are considered, some differences in the fundamental electrical parameters obtained from different methods can be observed. These differences arise from the dependence of the results on voltage and the calculation methods used. In other words, the TE theory, Cheung, and Norde models correspond to different voltage or current regions in the I-V data, and therefore, such variations are expected.

**Table 2:** Essential electrical parameters ($I_0$, $\Phi_{B0}$, n, $I_0$, $R_s$, $R_{sh}$, RR) and values obtained for Al/(CdO:ZnO:NiO:Ti)/p-Si/Al diodes for both dark and illumination under 100mW.cm$^{-2}$ at room temperature using Cheung&Cheung and Norde Method.

| | Cheung&Cheung Method | | | | Norde Method | |
|---|---|---|---|---|---|---|
| | n | $R_s$ (kΩ) | $\Phi_B$ (eV) | $R_s$ (kΩ) | $\Phi_B$ (eV) | $R_s$ (kΩ) |
| in dark | 11.25 | 2.827 | 0.687 | 2.462 | 0.653 | 2.679 |
| under 100 mW/cm$^2$ | 11.32 | 1.997 | 0.666 | 1.730 | 0.762 | 3.069 |

Both in Table 1 and Table 2 indicate an ideality factor higher than 1. It is quite common case in the literature previously Ilhan report et al report ideality factor values as 5.14 and 5.61 for $Cu_2FeSnS_4$ quaternary photodiodes. Ilhan et al also reported ideality factor for $Cu_2NiSnS_4$ diodes as 5.23 and 5.16. Koc reported the ideality factor as 3.97 for $Cu_2CoSnS_4$ photodiodes for IR illumination: Similarly, Ilhan report ideality factor of $Cu_2CoSnS_4$ photodetectors as 5.31 for 100mW/cm$^2$ illumination [34,46–48].

To determine the current conduction mechanisms, double-logarithmic $I_F$-$V_F$ graphs were obtained under both dark conditions and a light intensity of 100 mW·cm$^{-2}$, and these are presented in Figure 7. As seen in the figure, the ln($I_F$)-ln($V_F$) graph exhibits three distinct linear regions with different slopes under both dark and illuminated conditions. These regions correspond to low, medium, and high voltage ranges, respectively.

From the ln($I_F$)-ln($V_F$) curves, it is observed that the current follows the relation $I \sim V^m$, where m represents the slope of the linear regions, as indicated in the graph. As shown in Figure 7, these slopes vary approximately as $1 < V < 2V$, $2 < V < 3V$, and $3 < V < 6V$ for the low, medium, and high voltage regions, respectively. These values indicate that the current conduction mechanisms correspond to the Ohmic model in the low-voltage region, the space-charge limited current (SCLC) model in the medium-voltage region, and the trap-charge limited current (TCLC) model in the high-voltage region.

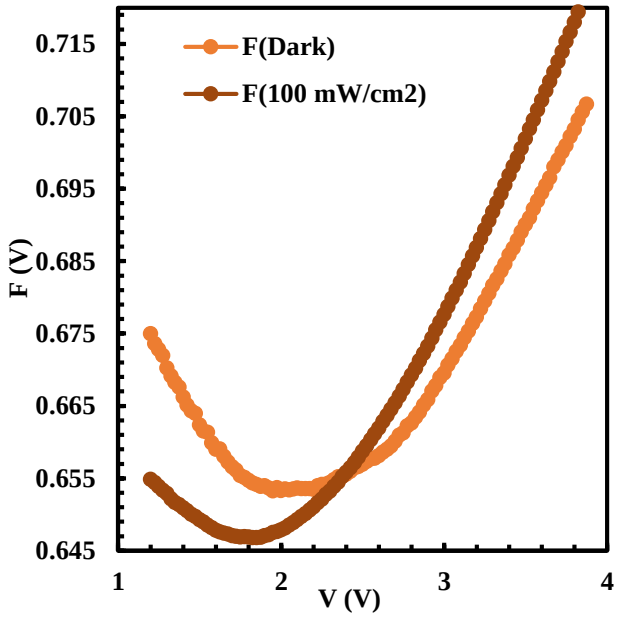


**Figure 6:** F(V)-V curves of Al/(CdO:ZnO:NiO:Ti)/p-Si/Al diode obtained in the dark and under 100mW.cm$^{-2}$ light intensity.

Using the forward bias $I_F$-$V_F$ data, the energy-dependent distribution profiles of the interface states ($N_{ss}$) as a function of ($E_c$-$E_{ss}$) were obtained for both dark conditions and under 100 mW/cm² illumination. These profiles were calculated by considering the voltage dependence of both the ideality factor and the potential barrier height, based on the equations developed by Card and Rhoderick, as provided below, and are presented in Figure 8 [38,39,49].

$$\Phi_e = \Phi_{B_0} + \alpha(V) = \Phi_{B_0} + \left(1 - \frac{1}{n(V)}\right)V \quad (9a)$$

$$E_{SS} - E_V = q(\Phi_e - V) \quad (9b)$$

$$N_{SS}(V) = \frac{1}{q}\left[\frac{\varepsilon_i}{d_i}(n(V) - 1) - \frac{\varepsilon_S}{W_D}\right] \quad (10)$$

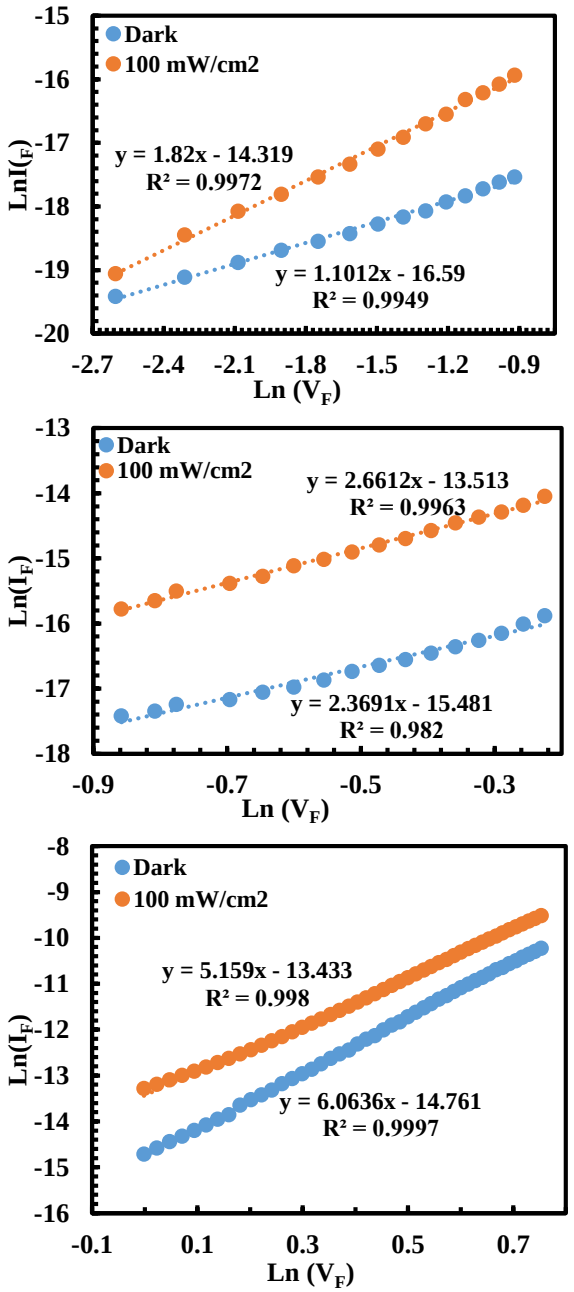


**Figure 7:** $\ln(I_F)$-$\ln(V_F)$ graphs for three different voltage regions of the Al/(CdO:ZnO:NiO:Ti)/p-Si/Al diode obtained in the dark and under 100mW/cm$^2$ light intensity.

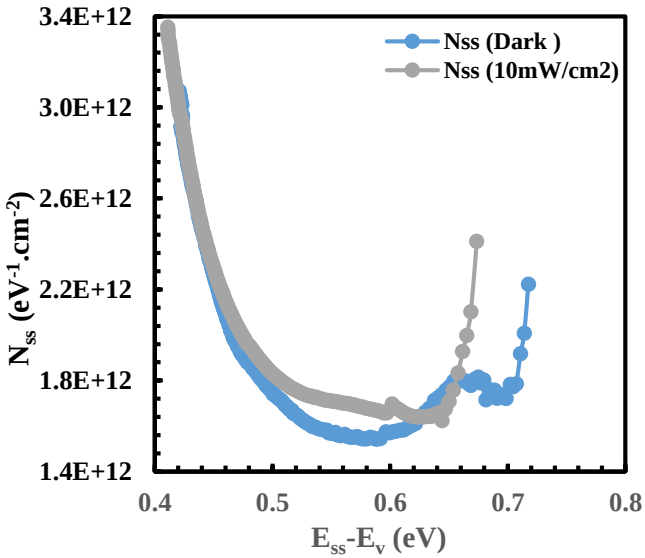


**Figure 8:** $N_{ss}$–($E_{ss}$-$E_V$) distribution profiles of Al/(CdO:ZnO:NiO:Ti)/p-Si/Al diode obtained in the dark and under 100mW.cm$^{-2}$ light.

Here, the α value represents the voltage coefficient of the measured barrier height and is a parameter that combines the effects of $N_{ss}$ with the equilibrium of the semiconductor.
As seen in Figure 8, the interface states exhibit a U-shaped distribution within the forbidden energy range, with values varying approximately between 1.3 × 10$^{12}$ eV$^{-1}$/cm$^2$ and 3.4 × 10$^{12}$ eV$^{-1}$/cm$^2$.

## 4. Conclusion

In this research, we focused on the fabrication and electrical characterization of Al/(CdO:ZnO:NiO:Ti)/p-Si/Al quaternary functional Schottky diodes, emphasizing their potential applications in optoelectronics. The thin films were produced using the sol-gel technique and characterized through current-voltage (I-V) measurements conducted in both dark and illuminated conditions. The findings revealed that the photodiodes exhibit notable photo responsive behaviour, positioning them as suitable candidates for light-sensitive applications such as photodetectors and solar cells. Key parameters such as barrier height ($\Phi_B$), ideality factor (n), series resistance ($R_s$), and shunt resistance ($R_{sh}$) were determined using various methods, including thermionic emission theory, Cheung & Cheung methods, and Norde techniques. Under dark conditions, the barrier height was recorded at 0.73 eV, which decreased to 0.69 eV when illuminated, indicating improved carrier transport in the presence of light. The ideality factors were found to be greater than one, measuring 9.61 in darkness and 8.78 under illumination, suggesting deviations from ideal behaviour attributed to the existence of interface states and interfacial layers. The values of series and shunt resistance, calculated through multiple models, exhibited consistent trends,

highlighting the influence of interfacial layers and trap states on diode performance. An analysis of double-logarithmic I-V plots revealed various current conduction mechanisms in different voltage ranges. This multi-region behaviour underscores the complexity of charge transport within these quaternary systems. Additionally, the study investigated the density of interface states ($N_{ss}$), which displayed U-shaped energy distribution patterns, further confirming the presence of trap states that impact device performance. The sensitivity of these parameters to illumination emphasizes the photodiodes' potential for applications that require light detection and energy harvesting.

In conclusion, Al/(CdO:ZnO:NiO:Ti)/p-Si/Al Schottky diodes exhibit promising electrical and optoelectronic properties, enhanced by the synergistic effects of their quaternary composition. Their photo responsive characteristics, coupled with adjustable electrical properties, make them strong candidates for advanced optoelectronic and photonic systems.

## References

[1] H. Frey H (2015) Applications and Developments of Thin Film Technology, in: Handbook of Thin-Film Technology. Springer Berlin Heidelberg, Berlin, Heidelberg. pp. 1–3. https://doi.org/10.1007/978-3-642-05430-3_1

[2] Karakuş E, Coşkun B (2023) A Brief Overview of Basic Surface Morphology Characterization Techniques in Thin Films. Journal of Materials and Electronic Devices 3 32–37. https://www.dergifytronix.com/index.php/jmed/article/view/264

[3] Krishnakumar T, Jayaprakash R, Prakash T, Sathyaraj D, Donato N, Licoccia S, Latino M, Stassi A, Neri G (2011) CdO-based nanostructures as novel $CO_2$ gas sensors. Nanotechnology 22 325501. https://doi.org/10.1088/0957-4484/22/32/325501

[4] Yıldırım M (2019) Characterization of the framework of Cu doped $TiO_2$ layers: An insight into optical, electrical and photodiode parameters. J Alloys Compd 773 890–904. https://doi.org/10.1016/j.jallcom.2018.09.276

[5] Yılmaz M, Tatar D, Sönmez E, Çırak C, Aydoğan S, Gunturkun R (2016) Investigation of Structural, Morphological, Optical, and Electrical Properties of Al Doped ZnO Thin Films Via Spin Coating Technique. Synthesis and Reactivity in Inorganic, Metal-Organic and Nano-Metal Chemistry 46 489–494. https://doi.org/10.1080/15533174.2014.988795

[6] Liddiard KC (1984) Thin-film resistance bolometer IR detectors. Infrared Phys 24 57–64. https://doi.org/10.1016/0020-0891(84)90048-4

[7] Yakuphanoğlu F, Çağlar Y, Çağlar M, Ilıcan S (2010) ZnO/p-Si heterojunction photodiode by solgel deposition of nanostructure n-ZnO film on p-Si substrate. Mater Sci Semicond Process 13 137–140. https://doi.org/10.1016/j.mssp.2010.05.005

[8] Mansour SA, Yakuphanoğlu F (2012) Electrical-optical properties of nanofiber ZnO film grown by sol gel method and fabrication of ZnO/p-Si heterojunction. Solid State Sci 14 121–126. https://doi.org/10.1016/J.SOLIDSTATESCIENCES.2011.11.007

[9] Yakuphanoğlu F (2011) Controlling of electrical and interface state density properties of ZnO:Co/p-silicon diode structures by compositional fraction of cobalt dopant. Microelectronics Reliability 51 2195–2199. https://doi.org/10.1016/j.microrel.2011.05.013

[10] Mekki A, Ocaya RO, Dere A, Al-Ghamdi AA, Harrabi K, Yakuphanoğlu F (2016) New photodiodes-based graphene-organic semiconductor hybrid materials. Synth Met 213 47–56. https://doi.org/10.1016/j.synthmet.2015.12.026

[11] Aslan F, Esen H, Yakuphanoğlu F (2019) Electrical and fotoconducting characterization of Al/coumarin:ZnO/Al novel organic-inorganic hybrid photodiodes. J Alloys Compd 789 595–606. https://doi.org/10.1016/j.jallcom.2019.03.090

[12] Kirsoy A, Ahmetoğlu M, Okutan M, Yakuphanoğlu F (2016) Electrical properties inorganic-on-organic hybrid GaAs/graphene oxide Schottky barrier diode. Journal of Nanoelectronics and Optoelectronics 11 108–114. https://doi.org/10.1166/JNO.2016.1884

[13] Ma XJ, Bin Zhang W, Bin Kong L, Luo YC, Kang L (2016) β-$Bi_2O_3$: An underlying negative electrode material obeyed electrode potential over electrochemical energy storage device. Electrochim Acta 192 45–51. https://doi.org/10.1016/j.electacta.2016.01.154

[14] Donati S (2001) Photodetectors: Devices, Circuits, and Applications. Meas Sci Technol 12 653. https://doi.org/10.1088/0957-0233/12/5/703

[15] Coşkun B (2020) Investigation of dielectric properties of Ag-doped ZnO thin films. J Mol Struct 1209 127970. https://doi.org/10.1016/J.MOLSTRUC.2020.127970

[16] Coşkun B (2019) Capacitance and Dielectric Properties of Mn Doped CdO Photodetectors. Journal of Materials and Electronic Devices 1 65–71.

[17] Coşkun ÖD, Zerrin T (2015) Optical, structural and bonding properties of diamond-like amorphous carbon films deposited by DC magnetron sputtering. Diam Relat Mater 56 29–35. https://doi.org/10.1016/J.DIAMOND.2015.04.004

[18] Yakuphanoğlu F, Okutan M, Korkmaz K (2008) The electrical conductivity and microstructure properties of Ni-doped $TiO_2$ ceramic. J Alloys Compd 450 39–43. https://doi.org/10.1016/j.jallcom.2006.10.117

[19] Farag AAM, Cavas M, Yakuphanoğlu F (2012) Electrical performance and interface states studies of undoped and Zn-doped CdO/p-Si heterojunction devices. Mater Chem Phys 132 550–558. https://doi.org/10.1016/j.matchemphys.2011.11.068

[20] Kurban M (2018) Size-and composition-dependent structure of ternary Cd-Te-Se nanoparticles. Turkish Journal of Physics 42 443–454. https://dergipark.org.tr/tr/pub/tbtkphysics/issue/40679/489952

[21] İlhan M, Koç MM, Coşkun B, Erkovan M, Yakuphanoğlu F (2021) Cd dopant effect on structural and optoelectronic properties of $TiO_2$ solar detectors. Journal of Materials Science: Materials in Electronics 32 2346–2365. https://link.springer.com/article/10.1007/s10854-020-05000-3

[22] Kılınç N, Sanduvac S, Erkovan M (2022) Platinum-Nickel alloy thin films for low concentration hydrogen sensor application. J Alloys Compd 892 162237. https://doi.org/10.1016/J.JALLCOM.2021.162237

[23] Erkovan M, Öcal MT, Öztürk O (2013) Tuning Magnetic Properties Polycrystalline of PtCo Alloys Films with Pt. Condensed Matter > Materials Science. https://doi.org/10.48550/arXiv.1401.0227

[24] Özden S, Koç MM (2018) Spectroscopic and microscopic investigation of MBE-grown CdTe (211) B epitaxial thin films on GaAs (211) B substrates, Appl Nanosci 8 891–903. https://doi.org/10.1007/s13204-018-0727-7

[25] Berberoğlu EA, Koç MM, Kurnaz Yetim N, Özcan C (2023) Removal of Highly Toxic Aqueous Cd2+ and Cr6+ Ions Using Dandelion-like $Co_3O_4$ Nanoflowers. Open Journal of Nano 8 36–49. https://doi.org/10.56171/OJN.1192105

[26] Uyar S, Coşkun B, İlhan M, Koç MM (2021) Optoelectronic Properties of ZnO:$TiO_2$ Nanocomposite Thin Films. Journal of Materials and Electronic Devices 5 21–27. https://dergi-fytronix.com/index.php/jmed/article/view/140

[27] Erkovan M, Shokr YA, Schiestl D, Wu CB, Kuch W (2015) Influence of NixMn1−x thickness and composition on the Curie temperature of Ni in NixMn1−x/Ni bilayers on Cu3Au (001). J Magn Magn Mater 373 151–154. https://doi.org/10.1016/J.JMMM.2014.02.017

[28] Aslan N, Koç MM, Dere A, Arif B, Erkovan M, Al-Sehemi AG, Al-Ghamdi AA, Yakuphanoğlu F (2018) Ti doped amorphous carbon (Al/Ti-a:C/p-Si/Al) photodiodes for optoelectronic applications. J Mol Struct 1155 813–818. https://doi.org/10.1016/j.molstruc.2017.11.050

[29] Roy UN, Camarda GS, Cui Y, James RB (2021) Advances in CdZnTeSe for Radiation Detector Applications. Radiation 2021, Vol. 1, Pages 123-130 1 123–130. https://doi.org/10.3390/RADIATION1020011

[30] Hwang S, Yu H, Bolotnikov AE, James RB, Kim K (2019) Anomalous Te Inclusion Size and Distribution in CdZnTeSe. IEEE Trans Nucl Sci 66 2329–2332. https://doi.org/10.1109/TNS.2019.2944969

[31] Chi W, Banerjee SK (2023) Comparison and integration of CuInGaSe and perovskite solar cells. Journal of Energy Chemistry 78 463–475. https://doi.org/10.1016/J.JECHEM.2022.12.039.

[32] Chandran R, Panda SK, Mallik A (2018) A short review on the advancements in electroplating of $CuInGaSe_2$ thin films. Materials for Renewable and Sustainable Energy 2018 7:2 7 1–20. https://doi.org/10.1007/S40243-018-0112-1

[33] Rondiya S, Wadnerkar N, Jadhav Y, Jadkar S, Haram S, Kabir M (2017) Structural, Electronic, and Optical Properties of $Cu_2NiSnS_4$: A Combined Experimental and Theoretical Study toward Photovoltaic Applications. Chemistry of Materials 29 3133–3142. https://doi.org/10.1021/acs.chemmater.7b00149

[34] İlhan M, Koç MM (2020) Infrared Sensing Properties of Quaternary $Cu_2CoSnS_4$ Photodetectors. Journal of Materials and Electronic Devices 1 19–24.

[35] Kaygılı O, Keser S, Ateş T, Al-Ghamdi AA, Yakuphanoğlu F (2013) Controlling of dielectrical and optical properties of hydroxyapatite based

bioceramics by Cd content. Powder Technol 245 1–6. https://doi.org/10.1016/j.powtec.2013.04.012.

[36] Yahia IS, Salem GF, Iqbal J, Yakuphanoğlu F (2017) Linear and nonlinear optical discussions of nanostructured Zn-doped CdO thin films. Physica B Condens Matter 511 54–60. https://doi.org/10.1016/J.PHYSB.2017.01.030

[37] Özden S, Koç MM (2019) Wet-chemical etching of GaAs (211) B wafers for controlling the surface properties. International Journal of Surface Science and Engineering 13 79. https://doi.org/10.1504/IJSURFSE.2019.102359

[38] Sharma B (1984) Metal-Semiconductor Schottky Barrier Junctions and Their Applications, Plenum Press, New York.

[39] Tung RT (2001) Recent advances in Schottky barrier concepts. Materials Science and Engineering: R: Reports 35 1–138. https://doi.org/10.1016/S0927-796X(01)00037-7

[40] Sze SM, Li Y, Kwok K Ng (2021) Physics of semiconductor devices. John Wiley & Sons, Inc., Hsinchu.

[41] Cheung SK, Cheung NW (1986) Extraction of Schottky diode parameters from forward current-voltage characteristics. Appl Phys Lett 49 85–87. https://doi.org/10.1063/1.97359

[42] Tataroğlu A, Altındal Ş (2008) Analysis of electrical characteristics of Au/$SiO_2$/n-Si (MOS) capacitors using the high-low frequency capacitance and conductance methods. Microelectron Eng 852256–2260. https://doi.org/10.1016/j.mee.2008.07.001

[43] Oruç Ç, Erkol A, Altındal A (2016) Conduction Mechanisms in Organic-based Rectifying Diode. Anadolu University Journal of Science and Technology A - Applied Sciences and Engineering 17 717–723. https://doi.org/10.18038/AUBTDA.267118.

[44] Altındal Yerişkin S, Balbaşı M, Orak İ (2017) The effects of (graphene doped-PVA) interlayer on the determinative electrical parameters of the Au/n-Si (MS) structures at room temperature. Journal of Materials Science: Materials in Electronics 28 14040–14048. https://doi.org/10.1007/S10854-017-7255-1

[45] Altındal Yerişkin S, Dere A, Orman Y, Yakuphanoğlu F (2024) Quaternary functional semiconductor devices. Phys Scr 99 075958. https://doi.org/10.1088/1402-4896/AD4F30

[46] İlhan M, Koç MM, Coşkun B, Yakuphanoğlu F (2020) Optical, Electrical and Photo responsive Properties of $Cu_2NiSnS_4$ Solar Detectors. J Electron Mater 49 4457–4465. https://doi.org/10.1007/s11664-020-08197-5

[47] İlhan M, Koç MM, Coşkun B, Dere A, Yakuphanoğlu F (2020) Structural and optoelectronic characterization of $Cu_2CoSnS_4$ quaternary functional photodetectors. Optik (Stuttg) 212 164724. https://doi.org/10.1016/j.ijleo.2020.164724

[48] İlhan M, Koç MM (2020) Infrared Detecting Behaviours of $Cu_2NiSnS_4$ photodiodes. Kırklareli Üniversitesi Mühendislik ve Fen Bilimleri Dergisi 6 119–131. https://doi.org/10.34186/klujes.702575.

[49] Rhoderick EH, Williams RH (1988) Metal-semiconductor contacts, 2nd ed.